Direct boundary integral equation method for electromagnetic scattering by partly coated dielectric objects

Originally published in:
Computing and Visualization in Science 8(3-4), https://doi.org/10.1007/s00791-005-0007-4

Comput Visual Sci (2005) 8: 145–158
DOI 10.1007/s00791-005-0007-4

Computing and Visualization in Science

REGULAR ARTICLE

B. Cranganu-Cretu · R. Hiptmair

Direct boundary integral equation method for electromagnetic scattering by partly coated dielectric objects

Received: 28 May 2004 / Accepted: 26 October 2004 / Published online: 1 December 2005

Communicated by: W. L. Wendland

Abstract We present a new variational direct boundary integral equation approach for solving the scattering and transmission problem for dielectric objects partially coated with a PEC layer. The main idea is to use the electromagnetic Calderón projector along with transmission conditions for the electromagnetic fields. This leads to a symmetric variational formulation which lends itself to Galerkin discretization by means of divergence-conforming discrete surface currents. A wide array of numerical experiments confirms the efficacy of the new method.

Keywords Electromagnetic scattering · Direct boundary integral equations · Galerkin boundary element method (BEM)

1 Introduction

A dielectric object (scatterer) of finite extension occupies the region Ω_s of three-dimensional space. Its surface $\Gamma := \partial\Omega_s$ is supposed to be piecewise smooth and Lipschitz-continuous: Ω_s is a curvilinear Lipschitz polyhedron in the parlance of [14]. This assumption will hold for all relevant CAD-generated geometries in industrial applications. We can distinguish two parts of the surface: a connected part Γ_0 coated with a thin metallic "mirror" layer that can be regarded as perfectly conducting, and a non-coated part Γ_a, the so-called aperture(s), see Fig. 1. The latter part is to consist of a few connected components, whose closures in Γ are disjoint. Moreover the common boundary of Γ_0 and Γ_a is assumed to be a union of curvilinear Lipschitz polygons.

The object is composed of a linear, homogeneous, isotropic material with dielectric constant ϵ_s and permeability μ_s. Outside, in the "air region" $\Omega' := \mathbb{R}^3 \setminus \overline{\Omega}_s$, we assume the electric properties of empty space. The scatterer is illuminated by a time harmonic plane wave of angular frequency $\omega > 0$. Since all fields will exhibit the same harmonic dependence on time, the scattering problem can be modeled in the frequency domain. Hence, the unknown quantities will be complex amplitudes (phasors). Those of the exciting electric and magnetic field read

$$\mathbf{e}_i(\mathbf{x}) = \mathbf{p}\,\exp(i\mathbf{k}\cdot\mathbf{x})\,,$$
$$\mathbf{h}_i(\mathbf{x}) = \frac{1}{\omega\mu}\,\mathbf{k}\times\mathbf{p}\,\exp(i\mathbf{k}\cdot\mathbf{x})\,. \tag{1}$$

Here $\mathbf{k} \in \mathbb{R}^3$ determines the propagation direction and $\mathbf{p}$ is the polarization of this *incident wave* [12, Sect. 6.6].

What we have described above is an *electromagnetic compatibility problem*, if the PEC coating is viewed as a shielding layer pierced at the aperture(s). We are interested to what extent the incident wave will penetrate through Γ_a and trigger electromagnetic fields inside Ω_s. Quantitative information about their strength at points in Ω_s has to be provided by numerical simulation.

A typical arrangement that fits the above abstract setting is provided by a metal container filled with a fluid. Some parts of the container's wall have been removed and replaced by glass or plastics, i.e., "windows", that do not interfere with the propagation of electromagnetic waves.

In the setting outlined above it is natural to employ a boundary integral equation method, which transforms the field equations in space to integral equations on Γ. This approach can easily accommodate the unbounded exterior air region and relieves us from meshing Ω_s and Ω'. These advantages account for the huge popularity of boundary integral equation methods for the simulation of electromagnetic scattering in the frequency domain [12, 37]. Even if the scatterer is not perfectly homogeneous, which rules out the use of a pure boundary element method, coupling of boundary elements and finite elements remains an attractive option [1, 23].

Boundary integral equation methods come in many different flavors: direct and indirect formulations and their

Dedicated to George C. Hsiao on the occasion of his 70th birthday.

B. Cranganu-Cretu
ABB Corporate Research, CH-5405 Baden-Dättwil, Switzerland
R. Hiptmair (✉)
SAM, ETH Zürich, CH-8092 Zürich, Switzerland
E-mail: hiptmair@sam.math.ethz.ch

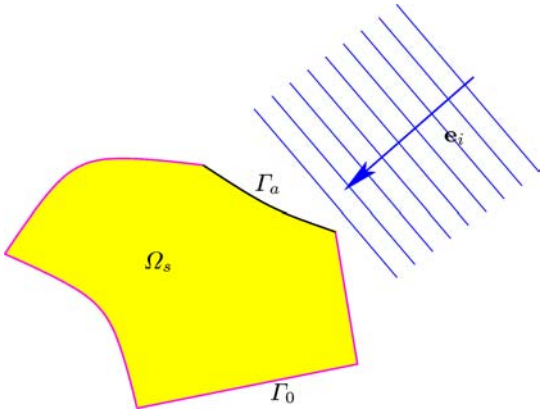

Fig. 1 Cross-section of a partly coated dielectric object

discretization based on the Nyström technique, collocation or a Galerkin approach. We are going to focus on Galerkin boundary element discretization of a direct boundary integral equation. The main reasons are

- that the direct method features tangential components of electromagnetic fields as primary unknowns, the very same quantities that occur in the transmission conditions across the aperture.
- that the structure of the resulting discretized equation perfectly matches the inherent symmetry of the coupled scattering problem. This paves the way for theoretical analysis.

We are not the first to tackle the aperture problem outlined above numerically (see [36] and the references cited therein). Approaches based on expansion into spherical harmonics are presented in [24, 32]. However, this only works for very special geometries. More flexibility is offered by the scheme proposed in [36], which is based on the equivalence principle [19]. Yet, this methods is of little practical value, because it entails inverting a large dense matrix. A fairly comprehensive presentation of indirect integral equation formulations is given in [21].

In this article we outline an approach that is based the Poincaré-Steklov operators associated with Maxwell's equations in free space. These operators are also known as the electric-to-magnetic mappings. They will be expressed through boundary integral operators and give rise to a coupled variational problem featuring traces of the electric and magnetic field on Γ as unknowns.

Our focus will be on both the derivation of the coupled variational problem and its Galerkin discretization and the performance of the resulting scheme in numerical experiments. We will sketch the theoretical justification for the validity of the coupled problem, but details will be skipped. A comprehensive exposure of the theoretical techniques is given in [8, 9].

2 Mathematical model

In the time-harmonic setting the behavior of the complex amplitudes of the electromagnetic fields in both Ω_s and Ω' is governed by the homogeneous Maxwell equations. Across the aperture Γ_a the usual continuity of tangential components of electric and magnetic field have to be enforced, whereas the tangential component of the electric field phasor vanishes on Γ_0. The model is summed up in the *transmission problem*, [26, Sect. 5.6.3]

$$\mathbf{curl}\ \mathbf{e} = -i\omega\mu\mathbf{h},\ \mathbf{curl}\ \mathbf{h} = i\omega\epsilon\mathbf{e}\ \text{ in } \Omega_s \cup \Omega', \tag{2}$$

$$\gamma_{\mathbf{t}}^{+}\mathbf{e} = 0,\ \gamma_{\mathbf{t}}^{-}\mathbf{e} = 0\ \text{ on } \Gamma_0, \tag{3}$$

$$\gamma_{\mathbf{t}}^{+}\mathbf{e} - \gamma_{\mathbf{t}}^{-}\mathbf{e} = -\gamma_{\mathbf{t}}^{+}\mathbf{e}_i,\ \gamma_{\mathbf{t}}^{+}\mathbf{h} - \gamma_{\mathbf{t}}^{-}\mathbf{h} = -\gamma_{\mathbf{t}}^{+}\mathbf{h}_i \text{ on } \Gamma_a, \tag{4}$$

$$\lim_{|\mathbf{x}|\to\infty} \mathbf{h}\times\mathbf{x} + |\mathbf{x}|\mathbf{e} = 0 \quad \text{uniformly.} \tag{5}$$

Here $\epsilon = \epsilon_0$, $\mu = \mu_0$ in Ω', and $\epsilon = \epsilon_s$, $\mu = \mu_s$ in Ω_s, that is, the material parameters are assumed to be constant also inside Ω_s. This is prerequisite for the boundary element techniques discussed in this paper.

Moreover, we write $\mathbf{n}$ for the unit normal vectorfield pointing from Ω_s into Ω' and $\gamma_{\mathbf{t}}\mathbf{u}$ for the tangential trace $\mathbf{u}\times\mathbf{n}$ of a vectorfield $\mathbf{u}$ on Γ, with superscripts $+$ and $-$ indicating that the trace is taken from Ω' or Ω_s, respectively.

Note that $\mathbf{e}$ and $\mathbf{h}$ stand for the *scattered fields* in Ω': the total fields are obtained by adding the incident wave fields $\mathbf{e}_i$ and $\mathbf{h}_i$, respectively. The scattered fields have to satisfy the Silver-Müller radiation conditions (5). As a consequence of Rellich's lemma and the unique continuation principle, the transmission problem (2)–(5) has a unique solution [10, 20].

Introducing the *wave numbers* (with physical unit m^{-1})

$$\kappa_- = \omega\sqrt{\epsilon_s\mu_s}\,, \qquad \kappa_+ = \omega\sqrt{\epsilon_0\mu_0}\,, \tag{6}$$

and eliminating the magnetic fields altogether, we end up with the electric wave equations

$$\mathbf{curl}\ \mathbf{curl}\ \mathbf{e} - \kappa_{\pm}^2\mathbf{e} = 0 \quad \text{in } \Omega'/\Omega_s, \text{ respectively.} \tag{7}$$

Due to the elimination of $\mathbf{h}$ we have to resort to the *magnetic trace operator*, $\gamma_N^{\pm} := \kappa^{-1}\gamma_{\mathbf{t}}^{\pm}\circ\mathbf{curl}$, which is related to tangential traces of the magnetic field. Traces of Maxwell solutions will be given a special name

Definition 1 Two tangential vectorfields $\boldsymbol{\xi}, \boldsymbol{\lambda}$ on Γ are called (interior/exterior) *Maxwell-Cauchy data*, if $\boldsymbol{\xi} = \gamma_{\mathbf{t}}^{\pm}\mathbf{u}$, $\boldsymbol{\lambda} = \gamma_N^{\pm}\mathbf{u}$, where $\mathbf{u}$ solves (7) in Ω'/Ω_s, respectively.

In terms of wave numbers, electric field and magnetic traces, the *transmission conditions* at Γ_a become

$$\begin{aligned} &\gamma_{\mathbf{t}}^{+}\mathbf{e} - \gamma_{\mathbf{t}}^{-}\mathbf{e} = -\gamma_{\mathbf{t}}^{+}\mathbf{e}_i\,,\\ &\frac{\kappa_+}{\mu_0}\gamma_N^{+}\mathbf{e} - \frac{\kappa_-}{\mu_s}\gamma_N^{-}\mathbf{e} = -\gamma_{\mathbf{t}}^{+}\mathbf{h}_i \ \text{ on } \Gamma_a\,. \end{aligned} \tag{8}$$

A crucial tool will be the Maxwell Steklov-Poincaré operators T^- and T^+, that is, electric-to-magnetic mappings, that take tangential components of the electric field on Γ_a to the magnetic traces of the associated Maxwell solutions in Ω_s and Ω', respectively. In order to define them properly, we

have to establish a suitable framework of function spaces. For a more detailed discussion we refer to [8, Sect. 2] and the references cited therein.

The natural energy spaces for the electric wave Eq. (7) are

$$\begin{aligned}\boldsymbol{H}(\mathbf{curl};\Omega_s) &:= \{\mathbf{u}:\Omega_s\mapsto\mathbb{C}^3,\ \mathbf{u}\in\mathbf{L}^2(\Omega_s),\\ &\qquad \mathbf{curl}\,\mathbf{u}\in\{L^2(\Omega_s)\}\},\\ \boldsymbol{H}_{\mathrm{loc}}(\mathbf{curl};\Omega') &:= \{\mathbf{u}:\Omega'\mapsto\mathbb{C}^3,\ \mathbf{u}\in\mathbf{L}^2_{\mathrm{loc}}(\Omega')\\ &\qquad \mathbf{curl}\,\mathbf{u}\in\mathbf{L}^2_{\mathrm{loc}}(\Omega')\},\end{aligned}$$

where $H(\mathbf{curl};\Omega_s$ becomes a Hilbert space when equipped with the natural graph norm $\|\cdot\|_{\boldsymbol{H}(\mathbf{curl};\Omega_s)}$.

Let $B\subset\mathbb{R}^3$ be a "big box" such that $\overline{\Omega}_s\subset B$. Green's formula for the **curl**-operator reveals that the tangential traces $\gamma_{\mathbf{t}}^-:\boldsymbol{C}^\infty(\overline{\Omega}_s)\mapsto TL^2(\Gamma)$, $\gamma_{\mathbf{t}}^+:\boldsymbol{C}^\infty(\overline{\Omega'\cap B})\mapsto TL^2(\Gamma)$, $TL^2(\Gamma):=\{\phi\in(L^2(\Gamma))^3,\ \phi\cdot\mathbf{n}=0\}$, can be extended to continuous mappings $\gamma_{\mathbf{t}}^-:\boldsymbol{H}(\mathbf{curl};\Omega_s)\mapsto(\mathrm{H}^{-\frac12}(\Gamma))^3$ and $\gamma_{\mathbf{t}}^+:\boldsymbol{H}(\mathbf{curl};\Omega'\cap\mathrm{B})\mapsto(\mathrm{H}^{-\frac12}(\Gamma))^3$, respectively. Therefore,

$$\boldsymbol{H}_{\Gamma_0}(\mathbf{curl};\Omega_s):=\{\mathbf{u}\in\boldsymbol{H}(\mathbf{curl};\Omega_s),\ \gamma_{\mathbf{t}}^-\mathbf{u}=0\text{ on }\Gamma_0\}$$

defines a closed subspace of $\boldsymbol{H}(\mathbf{curl};\Omega_s)$.

The characterization of the range of $\gamma_{\mathbf{t}}^-$ and $\gamma_{\mathbf{t}}^+$, in other words, the issue of trace spaces for $\boldsymbol{H}(\mathbf{curl};\Omega)$, turns out to be a mathematical challenge. Only recently, a comprehensive answer even for non-smooth domains was given in [5–7]. We summarize the results in the following theorem:

Theorem 1 (Trace theorem for $\boldsymbol{H}(\mathbf{curl};\Omega)$) *. There is a Hilbert space $\boldsymbol{H}_\times^{-\frac12}(div_\Gamma,\Gamma)$ of "tangential vectorfields" on Γ such that $\gamma_{\mathbf{t}}^-:\boldsymbol{C}^\infty(\overline{\Omega}_s)\mapsto TL^2(\Gamma)$ and $\gamma_{\mathbf{t}}^+:\boldsymbol{C}^\infty(\overline{\Omega'\cap B})\mapsto TL^2(\Gamma)$ can be extended to* continuous *and* surjective *mappings $\gamma_{\mathbf{t}}^-:\boldsymbol{H}(\mathbf{curl};\Omega_s)\mapsto\boldsymbol{H}_\times^{-\frac12}(div_\Gamma,\Gamma)$ and $\gamma_{\mathbf{t}}^+:\boldsymbol{H}(\mathbf{curl};\Omega'\cap B)\mapsto\boldsymbol{H}_\times^{-\frac12}(div_\Gamma,\Gamma)$, respectively.*

Crucial is the self-duality of $\boldsymbol{H}_\times^{-\frac12}(\mathrm{div}_\Gamma,\Gamma)$: based on the bilinear anti-symmetric pairing

$$\langle\boldsymbol{\mu},\boldsymbol{\eta}\rangle_{\tau,\Gamma}:=\int_\Gamma(\boldsymbol{\mu}\times\mathbf{n})\cdot\boldsymbol{\eta}\,\mathrm{d}S\,,\qquad\boldsymbol{\mu},\boldsymbol{\eta}\in\boldsymbol{L}^2_{\mathbf{t}}(\Gamma)\,,\tag{9}$$

the following result can be shown:

Theorem 2 (Self-duality of $\boldsymbol{H}_\times^{-\frac12}(\mathbf{div}_\Gamma,\Gamma)$) *. The pairing $\langle\cdot,\cdot\rangle_{\tau,\Gamma}$ can be extended to a continuous bilinear form on $\boldsymbol{H}_\times^{-\frac12}(div_\Gamma,\Gamma)$. With respect to $\langle\cdot,\cdot\rangle_{\tau,\Gamma}$ the space $\boldsymbol{H}_\times^{-\frac12}(div_\Gamma,\Gamma)$ becomes its own dual.*

Since the aperture Γ_a is a special part of the boundary, we need the results of [6] about traces of functions in $\boldsymbol{H}(\mathbf{curl};\Omega)$ onto parts of the boundary. We write $\mathbf{r}_a$ for the restriction operator $TL^2(\Gamma)\mapsto TL^2(\Gamma_a)$. Following [6, Sect. 5] we define

$$\begin{aligned}\boldsymbol{H}_{\times,00}^{-\frac12}(\mathrm{div}_\Gamma,\Gamma_a) &:= \mathbf{r}_a(\boldsymbol{H}_\times^{-\frac12}(\mathrm{div}_\Gamma,\Gamma))\,,\\ \boldsymbol{H}_\times^{-\frac12}(\mathrm{div}_\Gamma,\Gamma_a) &:= \{\phi\in\boldsymbol{H}_{\times,00}^{-\frac12}(\mathrm{div}_\Gamma,\Gamma_a),\\ &\qquad \widetilde{\phi}\in\boldsymbol{H}_\times^{-\frac12}(\mathrm{div}_\Gamma,\Gamma)\}\,,\end{aligned}$$

where $\widetilde{\phi}$ is the extension by zero of ϕ on Γ. It turns out that $\boldsymbol{H}_\times^{-\frac12}(\mathrm{div}_\Gamma,\Gamma_a)$ is a trace space [6, Theorem 5.3]:

Theorem 3 *The tangential trace $\gamma_{\mathbf{t}}^-:\boldsymbol{C}^\infty(\overline{\Omega}_s)\mapsto TL^2(\Gamma)$ gives rise to a* continuous *and* surjective *mapping $\gamma_{\mathbf{t}}^-:\boldsymbol{H}_{\Gamma_0}(\mathbf{curl};\Omega_s)\mapsto\boldsymbol{H}_\times^{-\frac12}(div_\Gamma,\Gamma_a)$.*

The expected duality also holds [6, Property 5.2]:

Theorem 4 *The Hilbert spaces $\boldsymbol{H}_{\times,00}^{-\frac12}(div_\Gamma,\Gamma_a)$ and $\boldsymbol{H}_\times^{-\frac12}(div_\Gamma,\Gamma_a)$ are dual to each other with respect to the duality pairing $\langle\cdot,\cdot\rangle_{\tau,\Gamma_a}$ which emerges from $\langle\cdot,\cdot\rangle_{\tau,\Gamma}$ by restriction to Γ_a.*

Remark. The duality results of Theorems 2 and 4 seem to be of mere theoretical value. Yet, at second glance, they provide crucial hints on how to set up proper variational formulations. This will be elaborated below.

As announced above, we will now introduce the electric-to-magnetic mappings

$$\mathsf{T}^-:\begin{cases}\boldsymbol{H}_\times^{-\frac12}(\mathrm{div}_\Gamma,\Gamma_a)\mapsto\boldsymbol{H}_\times^{-\frac12}(\mathrm{div}_\Gamma,\Gamma)\,,\\ \boldsymbol{\zeta}\qquad\qquad\mapsto\gamma_N^-\mathbf{e}\,,\end{cases}\tag{10}$$

where

$$\mathbf{curl}\,\mathbf{curl}\,\mathbf{e}-\kappa_-^2\mathbf{e}=0\ \text{ in }\Omega_s\,,\quad\gamma_{\mathbf{t}}^-\mathbf{e}=\widetilde{\boldsymbol{\zeta}}\ \text{ on }\Gamma\,,\tag{11}$$

$\widetilde{\boldsymbol{\zeta}}$ being the trivial extension of $\boldsymbol{\zeta}$ to Γ, and

$$\mathsf{T}^+:\begin{cases}\boldsymbol{H}_\times^{-\frac12}(\mathrm{div}_\Gamma,\Gamma)\mapsto\boldsymbol{H}_\times^{-\frac12}(\mathrm{div}_\Gamma,\Gamma)\,,\\ \boldsymbol{\zeta}\qquad\qquad\mapsto\gamma_N^+\mathbf{e}\,,\end{cases}\tag{12}$$

where $\mathbf{e}$ satisfies the Silver-Müller radiation conditions (5) and

$$\mathbf{curl}\,\mathbf{curl}\,\mathbf{e}-\kappa_+^2\mathbf{e}=0\ \text{ in }\Omega'\,,\quad\gamma_{\mathbf{t}}^+\mathbf{e}=\boldsymbol{\zeta}\ \text{ on }\Gamma\,.\tag{13}$$

In the general context of elliptic boundary value problems, the operators $\mathsf{T}^\pm$ are also known as Steklov-Poincaré operators.

It is important to note that T^- is not necessarily well defined: If κ_-^2 coincides with a Dirichlet eigenvalue of the differential operator **curl curl**, then the boundary value problem (11) will not have a unique solution. So, whenever using T^- we will tacitly make the *assumption* that

the wave number κ_- does not coincide with the square root of an interior Dirichlet eigenvalue of **curl curl** in Ω_s. (14)

Using the transmission conditions (8) along with the definition of the electric-to-magnetic mapping, and setting $\boldsymbol{\zeta} := \gamma_{\mathbf{t}}^{-}\mathbf{e} \in \boldsymbol{H}_{\times}^{-\frac{1}{2}}(\mathrm{div}_\Gamma, \Gamma_a)$, gives us the equation

$$\mathbf{r}_a\left(\frac{\kappa_-}{\mu_s}\mathsf{T}^-\boldsymbol{\zeta} - \frac{\kappa_+}{\mu_0}\mathsf{T}^+(\boldsymbol{\zeta} - \gamma_{\mathbf{t}}^{+}\mathbf{e}_i) - \gamma_{\mathbf{t}}^{+}\mathbf{h}_i\right) = 0 \quad \text{in } \boldsymbol{H}_{\times,00}^{-\frac{1}{2}}(\mathrm{div}_\Gamma, \Gamma_a)\,. \tag{15}$$

We have emphasized that this equation is posed in $\boldsymbol{H}_{\times,00}^{-\frac{1}{2}}(\mathrm{div}_\Gamma, \Gamma_a)$ to elucidate that the dual space $\boldsymbol{H}_{\times}^{-\frac{1}{2}}(\mathrm{div}_\Gamma, \Gamma_a)$ provides the right test functions for a variational formulation. This finally reads: seek $\boldsymbol{\zeta} \in \boldsymbol{H}_{\times}^{-\frac{1}{2}}(\mathrm{div}_\Gamma, \Gamma_a)$ such that

$$\left\langle \tfrac{\kappa_-}{\mu_s}\mathsf{T}^-\boldsymbol{\zeta} - \tfrac{\kappa_+}{\mu_0}\mathsf{T}^+(\widetilde{\boldsymbol{\zeta}} - \gamma_{\mathbf{t}}^{+}\mathbf{e}_i), \boldsymbol{\mu}\right\rangle_{\tau,\Gamma_a} = \left\langle \gamma_{\mathbf{t}}^{+}\mathbf{h}_i, \boldsymbol{\mu}\right\rangle_{\tau,\Gamma_a} \quad \forall \boldsymbol{\mu} \in \boldsymbol{H}_{\times}^{-\frac{1}{2}}(\mathrm{div}_\Gamma, \Gamma_a)\,. \tag{16}$$

Strictly speaking, the restriction operator $\mathbf{r}_a$ should be put in front of T^- and T^+.

Corollary 1 *If assumption* (14) *is satisfied, then* $\boldsymbol{\zeta}$ *solves* (16) *if and only if it agrees with the tangential trace* $\gamma_{\mathbf{t}}^{-}$ *of the solution* $\mathbf{e}$ *of* (2)–(5) *on* Γ_a.

Proof Let $\boldsymbol{\zeta}$ solve (16) and let $\mathbf{e}$ be composed of the unique solutions of (11) (in Ω_s) and (13) (in Ω'). Then $\mathbf{e}$ satisfies the transmission and boundary conditions on Γ and solves (7). The variational equation (16) ensures the transmission conditions for the related magnetic field.

If we have a solution $\mathbf{e}$ of (2)–(5), then, as a consequence of the transmission conditions, $\boldsymbol{\zeta} := \mathbf{r}_a(\gamma_{\mathbf{t}}^{-}\mathbf{e})$ will solve (16).

3 Electromagnetic calderón projector

The starting point of the derivation of boundary integral equations are representation formulas involving potentials, that is, mappings of functions on Γ to functions on $\Omega_s \cup \Omega'$. Well known are the scalar and vectorial single layer potentials, whose integral representation is given by ($\mathbf{x} \notin \Gamma$)

$$\Psi_V^\kappa(\phi)(\mathbf{x}) := \int_\Gamma \phi(\mathbf{y}) E_\kappa(\mathbf{x}-\mathbf{y})\, dS(\mathbf{y})\,,$$
$$\boldsymbol{\Psi}_{\mathbf{V}}^\kappa(\boldsymbol{\mu})(\mathbf{x}) := \int_\Gamma \boldsymbol{\mu}(\mathbf{y}) E_\kappa(\mathbf{x}-\mathbf{y})\, dS(\mathbf{y})\,,$$

with the Helmholtz kernel

$$E_\kappa(\mathbf{x}-\mathbf{y}) := \frac{\exp(i\kappa|\mathbf{x}-\mathbf{y}|)}{4\pi|\mathbf{x}-\mathbf{y}|}\,.$$

It is shown in [8, Sect. 4] and [12, Sect. 6.2] that, if $\mathbf{e} \in \boldsymbol{H}_{\mathrm{loc}}(\mathbf{curl}; \Omega_s \cup \Omega')$ satisfies

$$\mathbf{curl}\,\mathbf{curl}\,\mathbf{e} - \kappa^2\mathbf{e} = 0 \quad \text{in } \Omega_s \cup \Omega'\,, \tag{17}$$

and the Silver-Müller radiation conditions, then the field $\mathbf{e}$ can be represented by the so-called Stratton-Chu formula: using the jump operator $[\cdot]_\Gamma$ defined by $[\gamma]_\Gamma := \gamma^+ - \gamma^-$ for some trace γ onto Γ, it reads

$$\mathbf{e}(\mathbf{x}) = -\boldsymbol{\Psi}_{DL}^\kappa([\gamma_{\mathbf{t}}\mathbf{e}]_\Gamma)(\mathbf{x}) - \boldsymbol{\Psi}_{SL}^\kappa([\gamma_N\mathbf{e}]_\Gamma)(\mathbf{x})\,, \quad \mathbf{x} \in \Omega_s \cup \Omega'\,, \tag{18}$$

where we have introduced the (electric) *Maxwell single layer potential* according to

$$\boldsymbol{\Psi}_{SL}^\kappa(\boldsymbol{\mu})(\mathbf{x}) := \kappa\boldsymbol{\Psi}_{\mathbf{V}}^\kappa(\boldsymbol{\mu})(\mathbf{x}) + \tfrac{1}{\kappa}\mathbf{grad}_{\mathbf{x}}\Psi_V^\kappa(\mathrm{div}_\Gamma\boldsymbol{\mu})(\mathbf{x})\,,\ \mathbf{x} \notin \Gamma\,, \tag{19}$$

and the (electric) *Maxwell double layer potential*

$$\boldsymbol{\Psi}_{DL}^\kappa(\boldsymbol{\mu})(\mathbf{x}) := \mathbf{curl}\, x\boldsymbol{\Psi}_{\mathbf{V}}^\kappa(\boldsymbol{\mu})(\mathbf{x})\,, \quad \mathbf{x} \notin \Gamma\,. \tag{20}$$

Both Maxwell potentials provide radiating solutions of (17). They also allow the application of electric and magnetic trace operators from both sides of Γ [8, Theorem 5]. This paves the way for defining the *boundary integral operators*

$$\mathbf{S}_\kappa := \left\{\gamma_{\mathbf{t}}\boldsymbol{\Psi}_{SL}^\kappa\right\}_\Gamma\,, \quad \mathbf{C}_\kappa := \left\{\gamma_{\mathbf{t}}\boldsymbol{\Psi}_{DL}^\kappa\right\}_\Gamma\,,$$

where $\{\cdot\}_\Gamma$ is the average $\{\gamma\}_\Gamma := \frac{1}{2}(\gamma^+ + \gamma^-)$ for some trace γ onto Γ. In fact, owing to the intrinsic symmetry of electric and magnetic fields in Maxwell's equations, we also have

$$\mathbf{S}_\kappa = \left\{\gamma_N\boldsymbol{\Psi}_{DL}^\kappa\right\}_\Gamma\,, \quad \mathbf{C}_\kappa = \left\{\gamma_N\boldsymbol{\Psi}_{SL}^\kappa\right\}_\Gamma\,.$$

The operators $\mathbf{S}_\kappa$ and $\mathbf{C}_\kappa$ furnish *continuous* mappings $\mathbf{S}_\kappa, \mathbf{C}_\kappa : \boldsymbol{H}_{\times}^{-\frac{1}{2}}(\mathrm{div}_\Gamma, \Gamma) \mapsto \boldsymbol{H}_{\times}^{-\frac{1}{2}}(\mathrm{div}_\Gamma, \Gamma)$, [8, Cor. 2].

From (18) it is clear that not all traces can be continuous across Γ. More precise information is provided by the jump relations [8, Theorem 7]

$$\left[\gamma_{\mathbf{t}}\boldsymbol{\Psi}_{SL}^\kappa\right]_\Gamma = \left[\gamma_N\boldsymbol{\Psi}_{DL}^\kappa\right]_\Gamma = 0\,,$$
$$\left[\gamma_N\boldsymbol{\Psi}_{SL}^\kappa\right]_\Gamma = \left[\gamma_{\mathbf{t}}\boldsymbol{\Psi}_{DL}^\kappa\right]_\Gamma = -\mathrm{Id}\,.$$

Now, let us apply the exterior and interior trace operators to the representation formula (18) and use the jump relations. This gives

$$\gamma_{\mathbf{t}}^{-}\mathbf{u} = \tfrac{1}{2}\gamma_{\mathbf{t}}^{-}\mathbf{u} + \mathbf{C}_\kappa(\gamma_{\mathbf{t}}^{-}\mathbf{u}) + \mathbf{S}_\kappa(\gamma_N^{-}\mathbf{u})\,,$$
$$\gamma_{\mathbf{t}}^{+}\mathbf{u} = \tfrac{1}{2}\gamma_{\mathbf{t}}^{+}\mathbf{u} - \mathbf{C}_\kappa(\gamma_{\mathbf{t}}^{+}\mathbf{u}) - \mathbf{S}_\kappa(\gamma_N^{+}\mathbf{u})\,,$$
$$\gamma_N^{-}\mathbf{u} = \mathbf{S}_\kappa(\gamma_{\mathbf{t}}^{-}\mathbf{u}) + \tfrac{1}{2}\gamma_N^{-}\mathbf{u} + \mathbf{C}_\kappa(\gamma_N^{-}\mathbf{u}),$$
$$\gamma_N^{+}\mathbf{u} = -\mathbf{S}_\kappa(\gamma_{\mathbf{t}}^{+}\mathbf{u}) + \tfrac{1}{2}\gamma_N^{+}\mathbf{u} - \mathbf{C}_\kappa(\gamma_N^{+}\mathbf{u}).$$

A concise way to write these formulae relies on the *Calderon projectors*, *c.f.* [9, Sect. 3.3], [15, Formula (29)], and [26, Sect. 5.5],

$$\mathbb{P}_\kappa^- := \begin{pmatrix} \frac{1}{2}\mathrm{Id} + \mathbf{C}_\kappa & \mathbf{S}_\kappa \\ \mathbf{S}_\kappa & \frac{1}{2}\mathrm{Id} + \mathbf{C}_\kappa \end{pmatrix}\,,$$
$$\mathbb{P}_\kappa^+ := \begin{pmatrix} \frac{1}{2}\mathrm{Id} - \mathbf{C}_\kappa & -\mathbf{S}_\kappa \\ -\mathbf{S}_\kappa & \frac{1}{2}\mathrm{Id} - \mathbf{C}_\kappa \end{pmatrix}\,. \tag{21}$$

By construction, the operators $\mathbb{P}_\kappa^-$, $\mathbb{P}_\kappa^+$: $\boldsymbol{H}_\times^{-\frac{1}{2}}(\mathrm{div}_\Gamma, \Gamma)^2 \mapsto \boldsymbol{H}_\times^{-\frac{1}{2}}(\mathrm{div}_\Gamma, \Gamma)^2$ are projectors, that is,

$$\mathbb{P}_\kappa^- \circ \mathbb{P}_\kappa^- = \mathbb{P}_\kappa^- , \quad \mathbb{P}_\kappa^+ \circ \mathbb{P}_\kappa^+ = \mathbb{P}_\kappa^+ . \tag{22}$$

Also note that $\mathbb{P}_\kappa^- + \mathbb{P}_\kappa^+ = \mathrm{Id}$ and that the range of $\mathbb{P}_\kappa^+$ coincides with the kernel of $\mathbb{P}_\kappa^-$ and vice versa. The next result promotes Calderon projectors to a pivotal role in the derivation of boundary integral equations, *c.f.* [35, Theorem 3.7].

Theorem 5 *The pair of functions* $(\boldsymbol{\zeta}, \boldsymbol{\mu}) \in \boldsymbol{H}_\times^{-\frac{1}{2}}(div_\Gamma, \Gamma) \times \boldsymbol{H}_\times^{-\frac{1}{2}}(div_\Gamma, \Gamma)$ *are interior or exterior Maxwell Cauchy data (of a radiating solution of* (17)*), if and only if they lie in the kernel of* $\mathbb{P}_\kappa^+$ *or* $\mathbb{P}_\kappa^-$*, respectively.*

4 Coupled boundary integral equations

Next, we aim to find expressions for the Poincaré-Steklov operators using the boundary integral operators $\mathbf{S}_\kappa$ and $\mathbf{C}_\kappa$ introduced in the previous section. First, we introduce the scaled traces

$$(\boldsymbol{\zeta}^+, \boldsymbol{\lambda}^+) = (\gamma_\mathbf{t}^+ \mathbf{e}, \tfrac{\kappa_+}{\mu_0}\gamma_N^+ \mathbf{e}) , \quad (\boldsymbol{\zeta}^-, \boldsymbol{\lambda}^-) = (\gamma_\mathbf{t}^- \mathbf{e}, \tfrac{\kappa_-}{\mu_s}\gamma_N^- \mathbf{e}) .$$

Note that $\boldsymbol{\lambda}^\pm$ agree with the tangential traces of the magnetic field.

With these notations the transmission conditions on Γ_a read

$$\boldsymbol{\zeta}^- = \boldsymbol{\zeta}^+ + \gamma_\mathbf{t}^+ \mathbf{e}_i \quad \text{in } \boldsymbol{H}_\times^{-\frac{1}{2}}(\mathrm{div}_\Gamma, \Gamma_a) , \tag{23}$$

$$\boldsymbol{\lambda}^- = \boldsymbol{\lambda}^+ + \gamma_\mathbf{t}^+ \mathbf{h}_i \quad \text{in } \boldsymbol{H}_{\times,00}^{-\frac{1}{2}}(\mathrm{div}_\Gamma, \Gamma_a) . \tag{24}$$

For the sake of completeness we note that

$$\boldsymbol{\zeta}^- = 0 , \quad \boldsymbol{\zeta}^+ = -\gamma_\mathbf{t}^+ \mathbf{e}_i \quad \text{on } \Gamma_0 .$$

From Thm. 5 we conclude that

$$\begin{pmatrix} -\frac{1}{2}\mathrm{Id} + \mathbf{C}_{\kappa_-} & \frac{\mu_s}{\kappa_-}\mathbf{S}_{\kappa_-} \\ \frac{\kappa_-}{\mu_s}\mathbf{S}_{\kappa_-} & -\frac{1}{2}\mathrm{Id} + \mathbf{C}_{\kappa_-} \end{pmatrix} \begin{pmatrix} \boldsymbol{\zeta}^- \\ \boldsymbol{\lambda}^- \end{pmatrix} = 0 , \tag{25}$$

$$\begin{pmatrix} -\frac{1}{2}\mathrm{Id} - \mathbf{C}_{\kappa_+} & -\frac{\mu_0}{\kappa_+}\mathbf{S}_{\kappa_+} \\ -\frac{\kappa_+}{\mu_0}\mathbf{S}_{\kappa_+} & -\frac{1}{2}\mathrm{Id} - \mathbf{C}_{\kappa_+} \end{pmatrix} \begin{pmatrix} \boldsymbol{\zeta}^+ \\ \boldsymbol{\lambda}^+ \end{pmatrix} = 0 . \tag{26}$$

Three different equivalent formulas for the operators T^- and T^+ can be extracted from these identities. We could use either the top or bottom equation of (25) and (26) and formally arrive at the *non-symmetric expressions*, e.g.,

$$\boldsymbol{\lambda}^- = \tfrac{\kappa_-}{\mu_s}\mathbf{S}_\kappa^{-1}\big(\tfrac{1}{2}\mathrm{Id} - \mathbf{C}_\kappa\big)\boldsymbol{\zeta}^- , \tag{27}$$

$$\boldsymbol{\lambda}^- = \tfrac{\kappa_-}{\mu_s}\big(-\tfrac{1}{2}\mathrm{Id} + \mathbf{C}_\kappa\big)^{-1}\mathbf{S}_\kappa\boldsymbol{\zeta}^- . \tag{28}$$

However, starting with the work of M. Costabel [13] on scalar second order elliptic boundary value problems, numerical analysts realized that fundamental structural properties of the Steklov-Poincaré operator are much better preserved in the variational context, if a *symmetric expression* by means of boundary integral operators is used. This insight made it possible to come up with new formulations for coupled acoustic and electromagnetic scattering problems [9, 23, 35].

First, we use the bottom equations in (25) and (26), and get

$$\boldsymbol{\lambda}^- = \Big(\tfrac{\kappa_-}{\mu_s}\mathbf{S}_{\kappa_-}\Big)\boldsymbol{\zeta}^- + \Big(\tfrac{1}{2}\mathrm{Id} + \mathbf{C}_{\kappa_-}\Big)\boldsymbol{\lambda}^- , \tag{29}$$

$$\boldsymbol{\lambda}^+ = \Big(-\tfrac{\kappa_+}{\mu_0}\mathbf{S}_{\kappa_+}\Big)\boldsymbol{\zeta}^+ + \Big(\tfrac{1}{2}\mathrm{Id} - \mathbf{C}_{\kappa_+}\Big)\boldsymbol{\lambda}^+ . \tag{30}$$

Then, we rely on (27) and (28) to eliminate the magnetic traces remaining on the right hand side:

$$\boldsymbol{\lambda}^- = \Big(\tfrac{\kappa_-}{\mu_s}\mathbf{S}_{\kappa_-} - \Big(\tfrac{1}{2}\mathrm{Id} + \mathbf{C}_{\kappa_-}\Big)\cdot \Big(\tfrac{\mu_s}{\kappa_-}\mathbf{S}_{\kappa_-}\Big)^{-1}\Big(-\tfrac{1}{2}\mathrm{Id} + \mathbf{C}_{\kappa_-}\Big)\Big)\boldsymbol{\zeta}^- , \tag{31}$$

$$\boldsymbol{\lambda}^+ = \Big(-\tfrac{\kappa_+}{\mu_0}\mathbf{S}_{\kappa_+} + \Big(\tfrac{1}{2}\mathrm{Id} - \mathbf{C}_{\kappa_+}\Big)\cdot \Big(\tfrac{\mu_0}{\kappa_+}\mathbf{S}_{\kappa_+}\Big)^{-1}\Big(-\tfrac{1}{2}\mathrm{Id} - \mathbf{C}_{\kappa_+}\Big)\Big)\boldsymbol{\zeta}^+ . \tag{32}$$

Strictly speaking, this formal manipulation is only valid, if the invertibility of both $\mathbf{S}_{\kappa_-}$ and $\mathbf{S}_{\kappa_+}$ is guaranteed. This is the case, when assumption (14) holds for both κ^- and κ^+, see [8, Theorem 10]. Summing up, we have the representations

$$\mathsf{T}^- := \tfrac{\kappa_-}{\mu_s}\mathbf{S}_{\kappa_-} - \Big(\tfrac{1}{2}\mathrm{Id} + \mathbf{C}_{\kappa_-}\Big)\cdot \Big(\tfrac{\mu_s}{\kappa_-}\mathbf{S}_{\kappa_-}\Big)^{-1}\Big(-\tfrac{1}{2}\mathrm{Id} + \mathbf{C}_{\kappa_-}\Big) , \tag{33}$$

$$\mathsf{T}^+ := -\tfrac{\kappa_+}{\mu_0}\mathbf{S}_{\kappa_+} + \Big(\tfrac{1}{2}\mathrm{Id} - \mathbf{C}_{\kappa_+}\Big)\cdot \Big(\tfrac{\mu_0}{\kappa_+}\mathbf{S}_{\kappa_+}\Big)^{-1}\Big(-\tfrac{1}{2}\mathrm{Id} - \mathbf{C}_{\kappa_+}\Big) . \tag{34}$$

As expected, these operators map continuously

$$\mathsf{T}^-, \mathsf{T}^+ : \boldsymbol{H}_\times^{-\frac{1}{2}}(\mathrm{div}_\Gamma, \Gamma) \mapsto \boldsymbol{H}_\times^{-\frac{1}{2}}(\mathrm{div}_\Gamma, \Gamma) .$$

In principle, we could simply plug (33) and (34) into the variational equation (16). However, the presence of inverse operators in the definitions of T^- and T^+ rules out this straightforward approach, because the resulting equation would not be amenable to a direct Galerkin discretization. The usual trick to avoid these undesirable inverses is to use (29) and (30) and switch to a mixed formulation. It amounts

to using (27) and (28), in the process undoing the derivation of (31) and (32)

$$\begin{aligned}
\mathsf{T}^-\boldsymbol{\zeta} &= \left(\tfrac{\kappa_-}{\mu_s}\mathbf{S}_{\kappa_-}\right)\boldsymbol{\zeta} + \left(\tfrac{1}{2}\mathrm{Id} + \mathbf{C}_{\kappa_-}\right)\boldsymbol{\lambda}^-,\\
\boldsymbol{\lambda}^- &:= -\left(\tfrac{\mu_s}{\kappa_-}\mathbf{S}_{\kappa_-}\right)^{-1}\left(-\tfrac{1}{2}\mathrm{Id} + \mathbf{C}_{\kappa_-}\right)\boldsymbol{\zeta}\,,\\
\mathsf{T}^+\boldsymbol{\zeta}^+ &= \left(-\tfrac{\kappa_+}{\mu_0}\mathbf{S}_{\kappa_+}\right)\boldsymbol{\zeta}^+ + \left(\tfrac{1}{2}\mathrm{Id} - \mathbf{C}_{\kappa_+}\right)\boldsymbol{\lambda}^+,\\
\boldsymbol{\lambda}^+ &:= \left(\tfrac{\mu_0}{\kappa_+}\mathbf{S}_{\kappa_+}\right)^{-1}\left(-\tfrac{1}{2}\mathrm{Id} - \mathbf{C}_{\kappa_+}\right)\boldsymbol{\zeta}^+\,,
\end{aligned}$$

where $\boldsymbol{\lambda}^-, \boldsymbol{\lambda}^+ \in \boldsymbol{H}_{\times}^{-\frac{1}{2}}(\mathrm{div}_\Gamma, \Gamma)$ can be regarded as auxiliary unknowns defined on all of Γ. Merging with (16) we end up with the equations

$$\begin{pmatrix}
\frac{\kappa_-}{\mu_s}\mathbf{S}_{\kappa_-} + \frac{\kappa_+}{\mu_0}\mathbf{S}_{\kappa_+} & \frac{1}{2}\mathrm{Id} + \mathbf{C}_{\kappa_-} & \frac{1}{2}\mathrm{Id} - \mathbf{C}_{\kappa_+}\\
-\frac{1}{2}\mathrm{Id} + \mathbf{C}_{\kappa_-} & \frac{\mu_s}{\kappa_-}\mathbf{S}_{\kappa_-} & 0\\
\frac{1}{2}\mathrm{Id} + \mathbf{C}_{\kappa_+} & 0 & \frac{\mu_0}{\kappa_+}\mathbf{S}_{\kappa_+}
\end{pmatrix}\begin{pmatrix}\boldsymbol{\zeta}\\ \boldsymbol{\lambda}^-\\ \boldsymbol{\lambda}^+\end{pmatrix}$$
$$= \begin{pmatrix}
\gamma_{\mathbf{t}}^+\mathbf{h}_i + \frac{\kappa_+}{\mu_0}\mathbf{S}_{\kappa_+}(\gamma_{\mathbf{t}}^+\mathbf{e}_i)\\
0\\
(\frac{1}{2}\mathrm{Id} + \mathbf{C}_{\kappa_+})(\gamma_{\mathbf{t}}^+\mathbf{e}_i)\,.
\end{pmatrix}$$

The first equation is posed in $\boldsymbol{H}_{\times,00}^{-\frac{1}{2}}(\mathrm{div}_\Gamma, \Gamma_a)$ (as before, we omitted the restriction operator $\mathbf{r}_a$), while the second and third equation live in $\boldsymbol{H}_{\times}^{-\frac{1}{2}}(\mathrm{div}_\Gamma, \Gamma)$. Recalling the dualities of Theorem 2 and Theorem 4 we arrive at the equivalent variational problem: seek $\boldsymbol{\zeta} \in \boldsymbol{H}_{\times}^{-\frac{1}{2}}(\mathrm{div}_\Gamma, \Gamma_a)$, $\boldsymbol{\lambda}^- \in \boldsymbol{H}_{\times}^{-\frac{1}{2}}(\mathrm{div}_\Gamma, \Gamma)$, $\boldsymbol{\lambda}^+ \in \boldsymbol{H}_{\times}^{-\frac{1}{2}}(\mathrm{div}_\Gamma, \Gamma)$ such that

$$\begin{aligned}
&\left\langle (\tfrac{\kappa_-}{\mu_s}\mathbf{S}_{\kappa_-})\boldsymbol{\zeta} + (\tfrac{\kappa_+}{\mu_0}\mathbf{S}_{\kappa_+})(\boldsymbol{\zeta} - \gamma_{\mathbf{t}}^+\mathbf{e}_i), \boldsymbol{\mu}\right\rangle_{\tau,\Gamma_a}\\
&+ \left\langle (\tfrac{1}{2}\mathrm{Id} + \mathbf{C}_{\kappa_-})\boldsymbol{\lambda}^-, \boldsymbol{\mu}\right\rangle_{\tau,\Gamma_a}\\
&- \left\langle (\tfrac{1}{2}\mathrm{Id} - \mathbf{C}_{\kappa_+})\boldsymbol{\lambda}^+, \boldsymbol{\mu}\right\rangle_{\tau,\Gamma_a} = \langle \gamma_{\mathbf{t}}^+\mathbf{h}_i, \boldsymbol{\mu}\rangle_{\tau,\Gamma_a}\,,\\
&\left\langle (-\tfrac{1}{2}\mathrm{Id} + \mathbf{C}_{\kappa_-})\boldsymbol{\zeta}, \tau\right\rangle_{\tau,\Gamma}\\
&+ \left\langle (\tfrac{\mu_s}{\kappa_-}\mathbf{S}_{\kappa_-})\boldsymbol{\lambda}^-, \tau\right\rangle_{\tau,\Gamma} = 0\,,\\
&\left\langle (\tfrac{1}{2}\mathrm{Id} + \mathbf{C}_{\kappa_+})\boldsymbol{\zeta}, \theta\right\rangle_{\tau,\Gamma}\\
&+ \left\langle (\tfrac{\mu_0}{\kappa_+}\mathbf{S}_{\kappa_+})\boldsymbol{\lambda}^+, \theta\right\rangle_{\tau,\Gamma} = \left\langle (\tfrac{1}{2}\mathrm{Id} + \mathbf{C}_{\kappa_+})\gamma_{\mathbf{t}}^+\mathbf{e}_i, \theta\right\rangle_{\tau,\Gamma}
\end{aligned} \tag{35}$$

for all $\boldsymbol{\mu} \in \boldsymbol{H}_{\times}^{-\frac{1}{2}}(\mathrm{div}_\Gamma, \Gamma_a)$, $\tau \in \boldsymbol{H}_{\times}^{-\frac{1}{2}}(\mathrm{div}_\Gamma, \Gamma)$, $\theta \in \boldsymbol{H}_{\times}^{-\frac{1}{2}}(\mathrm{div}_\Gamma, \Gamma)$.

Lemma 1 *The variational problem* (35) *has a unique solution* $(\zeta^-, \lambda^+, \lambda^-) \in \boldsymbol{H}_{\times}^{-\frac{1}{2}}(div_\Gamma, \Gamma_a) \times \boldsymbol{H}_{\times}^{-\frac{1}{2}}(div_\Gamma, \Gamma) \times \boldsymbol{H}_{\times}^{-\frac{1}{2}}(div_\Gamma, \Gamma)$, *provided that* κ^+ *does not coincide with an interior electric Maxwell eigenvalue of* Ω_s.

Proof We study a solution $(\boldsymbol{\zeta}, \boldsymbol{\lambda}^+, \boldsymbol{\lambda}^-)$ of the homogeneous system with $\gamma_{\mathbf{t}}^+\mathbf{e}_i =$ and $\gamma_{\mathbf{t}}^+\mathbf{h}_i = 0$. Then set

$$\begin{pmatrix}\widetilde{\boldsymbol{\zeta}}^+\\ \widetilde{\boldsymbol{\lambda}}^+\end{pmatrix} := \begin{pmatrix}\frac{1}{2}\mathrm{Id} - \mathbf{C}_{\kappa_-} & -\frac{\mu_s}{\kappa_-}\mathbf{S}_{\kappa_-}\\ -\frac{\kappa_-}{\mu_s}\widehat{\mathbf{S}}_{\kappa_-} & \frac{1}{2}\mathrm{Id} - \mathbf{C}_{\kappa_-}\end{pmatrix}\begin{pmatrix}\boldsymbol{\zeta}\\ \boldsymbol{\lambda}^-\end{pmatrix}, \tag{36}$$

$$\begin{pmatrix}\widetilde{\boldsymbol{\zeta}}^-\\ \widetilde{\boldsymbol{\lambda}}^-\end{pmatrix} := \begin{pmatrix}\frac{1}{2}\mathrm{Id} + \mathbf{C}_{\kappa_+} & \frac{\mu_0}{\kappa_+}\mathbf{S}_{\kappa_+}\\ \frac{\kappa_-}{\mu_0}\widehat{\mathbf{S}}_{\kappa_+} & \frac{1}{2}\mathrm{Id} + \mathbf{C}_{\kappa_+}\end{pmatrix}\begin{pmatrix}\boldsymbol{\zeta}\\ \boldsymbol{\lambda}^+\end{pmatrix}, \tag{37}$$

Please note that the operators in (36) and (37) are scaled versions of the Calderón projectors (21) that link genuine tangential traces of electric and magnetic fields. In particular, (36) is the scaled exterior Calderón projector for the interior wave number κ_-, and (37) provides the scaled interior Calderón projector for the exterior wave number κ_+.

This means that $\widetilde{\boldsymbol{\zeta}}^+, \widetilde{\boldsymbol{\lambda}}^+$ are exterior electric and magnetic tangential traces of some Maxwell solution, whereas $\widetilde{\boldsymbol{\zeta}}^-, \widetilde{\boldsymbol{\lambda}}^-$ turn out to be interior electric and magnetic traces, also of a Maxwell solution.

From the second and third equation of (35) with zero r.h.s. it is immediate that

$$\widetilde{\boldsymbol{\zeta}}^- = \widetilde{\boldsymbol{\zeta}^+} = 0\,.$$

Thus, the unique solvability of the exterior scattering problem yields $\widetilde{\boldsymbol{\lambda}}^+ = 0$. If κ_+ is different from an interior electric Maxwell eigenvalue, then we can also conclude $\boldsymbol{\lambda}^- = 0$. Hence, we have shown

$$\begin{aligned}
&\begin{pmatrix}\frac{1}{2}\mathrm{Id} + \mathbf{C}_{\kappa_-} & \frac{\mu_s}{\kappa_-}\mathbf{S}_{\kappa_-}\\ \frac{\kappa_-}{\mu_s}\widehat{\mathbf{S}}_{\kappa_-} & \frac{1}{2}\mathrm{Id} + \mathbf{C}_{\kappa_-}\end{pmatrix}\begin{pmatrix}\boldsymbol{\zeta}\\ \boldsymbol{\lambda}^-\end{pmatrix} = \begin{pmatrix}\boldsymbol{\zeta}\\ \boldsymbol{\lambda}^-\end{pmatrix},\\
&\begin{pmatrix}\frac{1}{2}\mathrm{Id} - \mathbf{C}_{\kappa_+} & -\frac{\mu_0}{\kappa_+}\mathbf{S}_{\kappa_+}\\ -\frac{\kappa_-}{\mu_0}\widehat{\mathbf{S}}_{\kappa_+} & \frac{1}{2}\mathrm{Id} - \mathbf{C}_{\kappa_+}\end{pmatrix}\begin{pmatrix}\boldsymbol{\zeta}\\ \boldsymbol{\lambda}^+\end{pmatrix} = \begin{pmatrix}\boldsymbol{\zeta}\\ \boldsymbol{\lambda}^+\end{pmatrix}.
\end{aligned}$$

This means that $\boldsymbol{\zeta}, \boldsymbol{\lambda}^-$ are electric and magnetic traces of a solution of the interior scattering problem with wave number κ_-, and $\boldsymbol{\zeta}, \boldsymbol{\lambda}^+$ play the same role for an exterior scattering problem with wave number κ_+.

Moreover, from the first equation of (35) we can infer that

$$\begin{aligned}
\boldsymbol{\lambda}^- - \boldsymbol{\lambda}^+ = &\left(\tfrac{\kappa_-}{\mu_s}\widehat{\mathbf{S}}_{\kappa_-} + \tfrac{\kappa_-}{\mu_0}\widehat{\mathbf{S}}_{\kappa_+}\right)\boldsymbol{\zeta} + \left(\tfrac{1}{2}\mathrm{Id} + \mathbf{C}_{\kappa_-}\right)\boldsymbol{\lambda}^-\\
&- \left(\tfrac{1}{2}\mathrm{Id} - \mathbf{C}_{\kappa_+}\right)\boldsymbol{\lambda}^+ = 0 \quad \text{on } \Gamma_a\,.
\end{aligned}$$

Summing up, the boundary data $(\boldsymbol{\zeta}, \boldsymbol{\lambda}^-, \boldsymbol{\lambda}^+)$ are the traces of the electric field and the magnetic field, respectively, that solve the scattering problem for the coated dielectric object Ω. Since we considered the case of zero excitation, the unique solvability of the scattering problem enforces $\boldsymbol{\zeta} = \boldsymbol{\lambda}^- = \boldsymbol{\lambda}^+ = 0$.

Remark. The assumption on κ^+ of the Lemma seems odd in light of assumption (14). Yet, taking into account the unique solvability of the transmission problem, both assumptions are undesirable. They are related to the phenomenon of

"forbidden frequencies" [16] or "spurious resonances" that haunt most variational formulations of scattering transmission problems. A profound analysis of the impact of spurious resonances in the case of electromagnetic scattering is given in [11].

In fact, when facing a spurious resonance, the solutions for $\boldsymbol{\lambda}^-$ in (35) may no longer be unique, but the fields recovered through the representation formula (18) will. Nevertheless, spurious resonances are worrisome, because they involve a loss of stability that will lead to singular or nearly singular linear systems after discretization.

An elegant way to avoid spurious resonances in the case of a purely exterior scattering problem are combined field integral equations [12, Ch. 3 & 6]. Unfortunately, an analogous stable formulation for the transmission problem has hitherto not been found.

Remark. The proof of existence of solutions for (35) hinges on a generalized Gårding inequality satisfied by the bilinear form underlying (35) and employs the Fredholm alternative. The technique is elaborated in [8, Sect. 7].

5 Galerkin boundary element discretization

We aim to use a conforming Galerkin boundary element discretization of (35). To that end, Γ will be approximated by a triangulation Γ_h composed of flat triangles. We assume that the boundary of Γ_a is approximately resolved by edges of Γ_h.

Next, we have to construct a finite dimensional subspaces $\boldsymbol{\mathcal{V}}_h \subset \boldsymbol{H}_{\times}^{-\frac{1}{2}}(\mathrm{div}_\Gamma, \Gamma_a)$ and $\boldsymbol{\mathcal{W}}_h \subset \boldsymbol{H}_{\times}^{-\frac{1}{2}}(\mathrm{div}_\Gamma, \Gamma)$ that contain piecewise polynomial surface vector fields and possess locally supported basis functions. To motivate their construction, we look at $\boldsymbol{H}(\mathbf{curl}; \Omega_s)$-conforming finite element schemes for the approximation of electric and magnetic fields. The simplest is provided by the so-called edge elements [22], also known as lowest order Nédélec finite elements [25]. Keeping in mind that $\boldsymbol{H}_{\times}^{-\frac{1}{2}}(\mathrm{div}_\Gamma, \Gamma) = \gamma_{\mathbf{t}}^-(\boldsymbol{H}(\mathbf{curl}; \Omega_s))$, see Theorem 3, we simply take the tangential traces of edge element functions on a mesh Ω_h with $\Omega_{h|\Gamma} = \Gamma_h$ as space $\boldsymbol{\mathcal{W}}_h$. This will give a space of piecewise linear vectorfields on Γ, whose "surface normal components" are continuous across edges of triangles. This is a well-known sufficient condition for $\boldsymbol{\mathcal{W}}_h \subset \boldsymbol{H}_{\times}^{-\frac{1}{2}}(\mathrm{div}_\Gamma, \Gamma)$. The local shape functions on a triangle T are given by the formula

$$\mathbf{b}_{i,j}^T := \lambda_i \mathbf{curl}_\Gamma \lambda_j - \lambda_j \mathbf{curl}_\Gamma \lambda_i \quad 1 \le i < j \le 3\,, \tag{38}$$

where λ_i, $i = 1, 2, 3$, are the local linear barycentric coordinate functions in T. These basis functions are sketched in Fig. 2. They are associated with the edges of Γ_h so that $\dim \boldsymbol{\mathcal{W}}_h$ will agree with the total number N of edges of Γ_h. Note that $\boldsymbol{\mathcal{W}}_h$ agrees with the lowest order div-conforming Raviart-Thomas elements in 2D, *cf.* [2, Ch. 3]. In electrical engineering $\boldsymbol{\mathcal{W}}_h$ is known as the space of Rao-Wilton-Glisson (RWG) boundary elements [27].

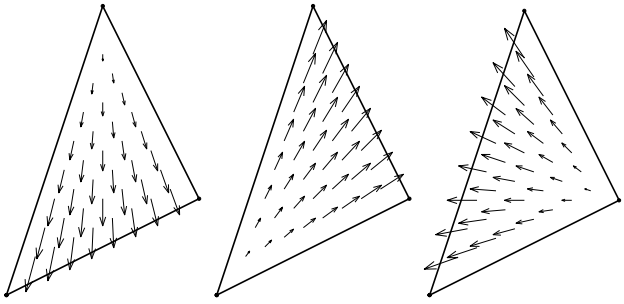

Fig. 2 Local shape functions of $\boldsymbol{\mathcal{W}}_h$

In order to find $\boldsymbol{\mathcal{V}}_h$ recall that an edge element subspace of $\boldsymbol{H}_{\Gamma_0}(\mathbf{curl}; \Omega_s)$ can be obtained by dropping all basis functions associated with edges on Γ_0. As $\boldsymbol{H}_{\times}^{-\frac{1}{2}}(\mathrm{div}_\Gamma, \Gamma_a) = \gamma_{\mathbf{t}}^- \boldsymbol{H}_{\Gamma_0}(\mathbf{curl}; \Omega_s)$, $\boldsymbol{\mathcal{V}}_h$ will be spanned by all basis functions (38) belonging to edges *in the interior* of Γ_a. Let N_a denote their number.

To compute the linear system of equations arising from the surface edge element discretization of (35) we need an explicit integral representation for the boundary integral operators $\mathbf{S}_\kappa$ and $\mathbf{C}_\kappa$: for $\boldsymbol{\mu}, \boldsymbol{\xi} \in (L^\infty(\Gamma))^3 \cap \boldsymbol{L}_{\mathbf{t}}^2(\Gamma)$ there holds [28]:

$$\begin{aligned}
&\langle \mathbf{S}_\kappa \boldsymbol{\mu}, \boldsymbol{\xi} \rangle_{\tau,\Gamma} \\
&= -\kappa \int_\Gamma \int_\Gamma E_\kappa(\mathbf{x}-\mathbf{y})\, \boldsymbol{\mu}(\mathbf{y}) \cdot \boldsymbol{\xi}(\mathbf{x})\, \mathrm{d}S(\mathbf{y}, \mathbf{x}) \\
&\quad + \frac{1}{\kappa} \int_\Gamma \int_\Gamma E_\kappa(\mathbf{x}-\mathbf{y})\, \mathrm{div}_\Gamma \boldsymbol{\mu}(\mathbf{y})\, \mathrm{div}_\Gamma \boldsymbol{\xi}(\mathbf{x})\, \mathrm{d}S(\mathbf{y}, \mathbf{x})\,, \qquad (39) \\
&\langle \mathbf{C}_\kappa \boldsymbol{\mu}, \boldsymbol{\xi} \rangle_{\tau,\Gamma} \\
&= -\int_\Gamma \int_\Gamma \mathbf{grad}_{\mathbf{x}} E_\kappa(\mathbf{x}-\mathbf{y}) \cdot (\boldsymbol{\mu}(\mathbf{y}) \times \boldsymbol{\xi}(\mathbf{x}))\, \mathrm{d}S(\mathbf{y}, \mathbf{x})\,. \qquad (40)
\end{aligned}$$

In the case of $\mathbf{S}_\kappa$ we encounter a weakly singular integral operator, whereas $\mathbf{C}_\kappa$ is Cauchy singular on non-smooth surfaces. Special quadrature techniques are required in order to evaluate $\mathbf{S}_\kappa$ and $\mathbf{C}_\kappa$ for pairs of basis functions (38). If the supports of the basis functions are disjoint ("far field") the evaluation will be based on a fixed quadrature rule that is exact for polynomials up to degree 5. Otherwise, in the case of overlapping or adjacent supports ("near field"), a technique making use of Duffy transforms is used [18, 30, 32]: By a suitable coordinate transformation an integral with an analytic integrand is obtained. For details we refer to [31, Ch. 5].

Eventually, the transmission problem has been converted into a square linear system for the $2N + N_a$ unknown coefficients corresponding to surface currents crossing edges of Γ_h: on $\overline{\Gamma_0}$ each edge bears two unknowns, each interior edge of Γ_a has three of them.

Remark. Surface edge elements enjoy a number of unique stability properties owed to their nature as discrete differential forms, see [8, Sect. 8] and [3]. This makes it possible to show the quasi-optimality of Galerkin solutions provided that the mesh Γ_h is fine enough [4].

6 Numerical experiments

The new discrete boundary integral formulation is tested numerically for several different arrangements, namely a metallic hollow sphere with a circular aperture, a metallic rectangular container, partially covered and filled with sea water, and, finally, a metallic box with one, two and four slots, respectively.

Throughout, the linear systems of equations arising from the boundary element Galerkin discretization were solved iteratively using GMRES for complex matrices [29]. Its termination criterion was a relative drop of the Euclidean norm of the residual by a factor of 10^4. This seemed to be sufficient to suppress any visible impact of the iteration's truncation error. Neither preconditioning nor acceleration of matrix-vector products by means of fast multipole techniques has been used, because the focus was on assessing the accuracy of the method.

Remark. All computations were done on rather uniform surface meshes consisting of flat triangles. Neither anisotropic elements nor local refinement was employed. However, we point out that, in fact, the use of anisotropic meshes graded toward the edge of the aperture is highly advisable.

Remark. In a series of experiments we used $\epsilon_s = \epsilon_0$ and $\mu_s = \mu_0$. In this case the problem boils down to scattering at a PEC screen and can be solved by means of the so-called electric field integral equation (EFIE) [4].

6.1 Metallic hollow sphere

We first investigated scattering at a metallic hollow sphere (radius 1m) that possesses a 60° circular aperture (angle

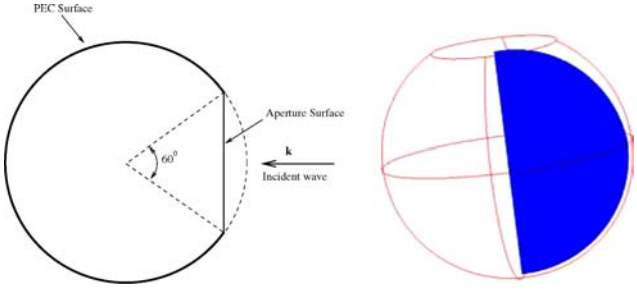

Fig. 3 Geometry of the first arrangement. The incident plane wave is propagating toward the aperture. Transmitted field computed on blue surface

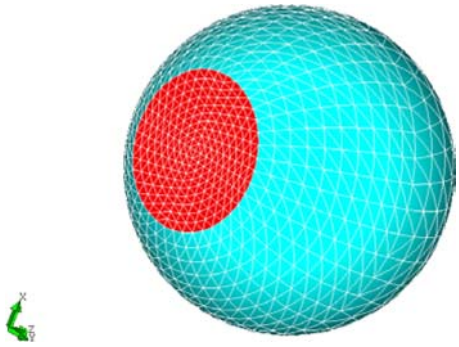

Fig. 4 Meshed geometry of the problem (medium sized mesh - 3440 unknowns). Cyan marks PEC coating, red the aperture

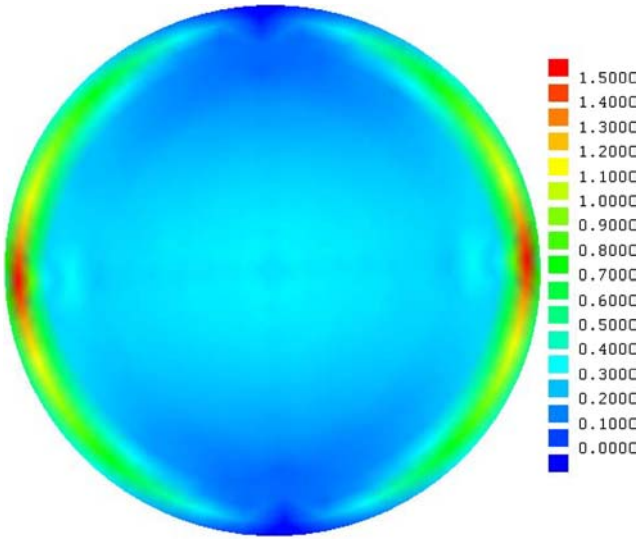

Fig. 5 Modulus of tangential electric field on the surface of the aperture [V/m]. Normalized wave number $\kappa = 2.75$

measured from the center of the sphere, see Fig. 3). The excitation is a plane wave, linearly polarized and propagating in positive $\mathbf{e}_z$-direction:

$$\mathbf{e}_i = \mathbf{p}\exp(-i\mathbf{k}\cdot\mathbf{x})\,,\quad \mathbf{k} = k\,\mathbf{e}_z\,,\quad \mathbf{p} = p\mathbf{e}_x\,,\quad p = 1\frac{\mathrm{V}}{\mathrm{m}}\,. \tag{41}$$

This type of excitation was used for all numerical tests. Both in the exterior and in the interior of the metallic sphere we have $\epsilon = \epsilon_0$, $\mu = \mu_0$.

We performed scattering simulations for various frequencies covering the first resonance (at $\kappa \approx 2.75\,\mathrm{m}^{-1}$). Note that, since Γ_a is flat, see Fig. 3, the actual interior resonant frequencies of Ω_s are expected to be slightly different from those of a perfect sphere.

For the approximate resonant wave number $\kappa \approx 2.75\,\mathrm{m}^{-1}$ we plotted the modulus of the tangential electric field in the aperture (Fig. 5) as well as of the modulus of the tangential magnetic field inside and outside of Γ_0 (Fig. 6 and Fig. 7). Figure 8 presents the modulus of the transmitted field on a surface parallel to the propagation direction (blue surface in Fig. 3). In all the plots smoothing and averaging was performed for the sake of visualization.

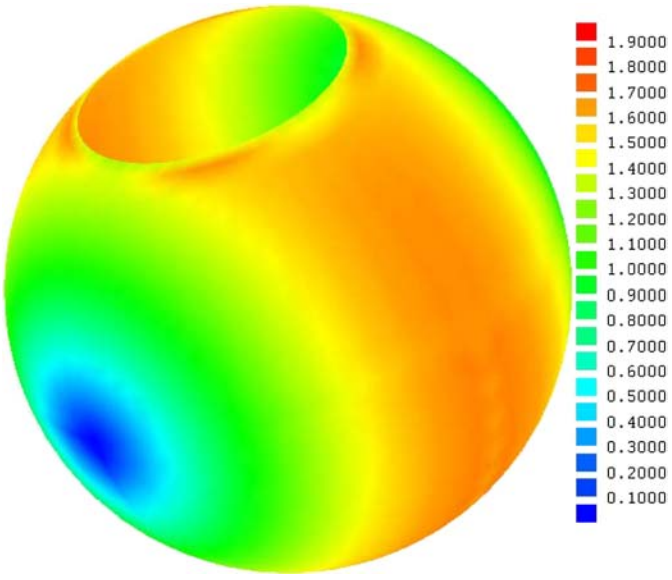

Fig. 6 Modulus of inner tangential magnetic field [A/m]. Normalized wave number k = 2.75

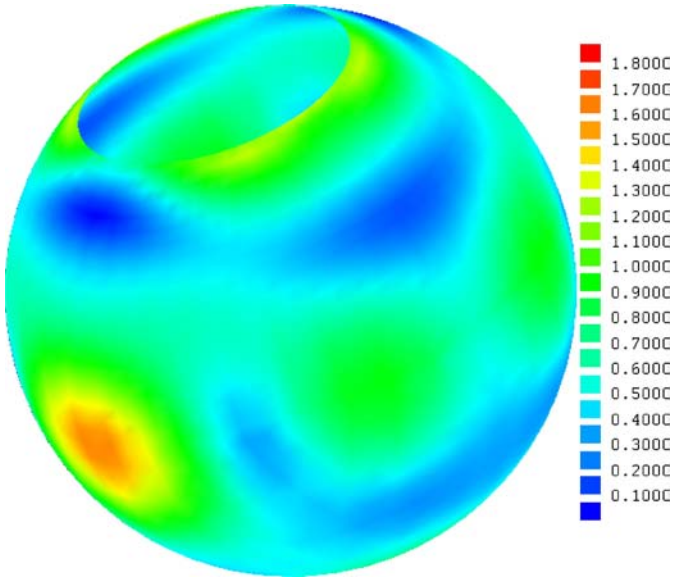

Fig. 7 Modulus of outer tangential magnetic field [A/m]. Normalized wave number $\kappa = 2.75$

We also performed a series of experiments to assess the convergence of the Galerkin solutions. To that end we relied on three meshes ranging from coarse (800 unknowns) to fine (5400 unknowns). The results are presented in Fig. 9, which hints at convergence to a limit solution.

For a discretization comprising 5400 unknowns the scattering simulation was carried out for various wave numbers around the first resonance of the configuration. The results are presented in Fig. 10 (To avoid problems arising from singular integrals the representation formula was not evaluated very close to Γ.).

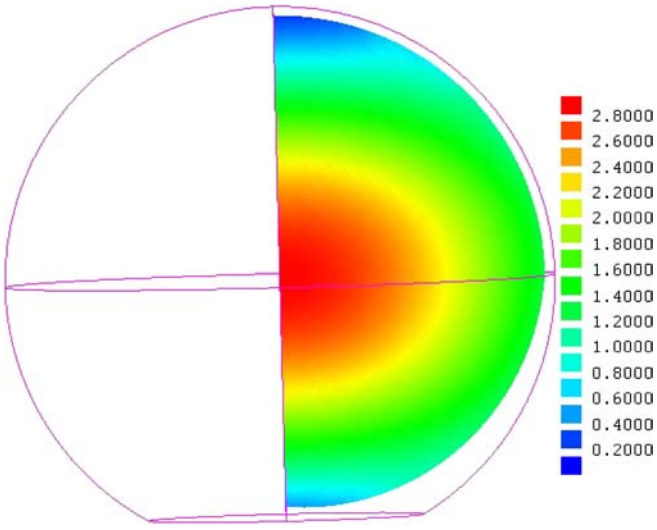

Fig. 8 Modulus of transmitted electric field [V/m]. Wave number $\kappa = 2.75$

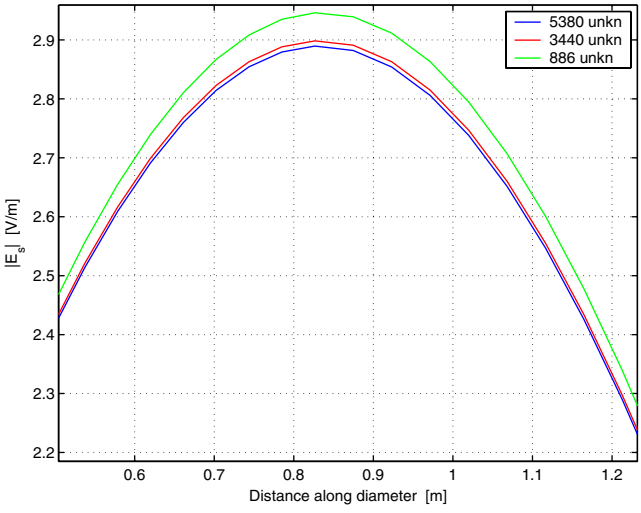

Fig. 9 Sphere: influence of mesh refinement on accuracy of solution. E_s: modulus of total electric field **e** along diametrical line

Figure 11 presents results for the electric field shielding factor (EFS) at a point $\mathbf{x} \in \Omega_s$, computed according to

$$EFS(\mathbf{x}) = -20 \log \left| \frac{\mathbf{e}(\mathbf{x})}{\mathbf{e}_i(\mathbf{x})} \right| \ [\text{dB}] \ . \tag{42}$$

Here, **x** was the center of the sphere.

We compared the results obtained by the new coupled boundary element method with the quasi-analytical formulation used by Senior and Desjardins in [33] (for the sphere with circular aperture), see Fig. 12. A maximum relative difference of 7.6 % is observed.

Finally we considered several different angles of incidence of the plane wave on the plane of the aperture. The angle was measured between the wave vector **k** and $-\mathbf{e}_z$ (normal to aperture). The results are presented in Fig. 13

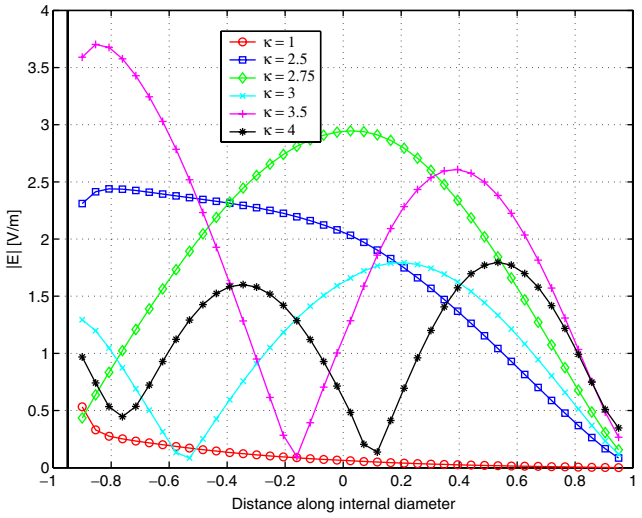

Fig. 10 Sphere: scattered (transmitted) field along diameter for different incident wave around first resonance of the complete sphere. Left vertical line—aperture surface, PEC surface at 1.0 on abscissa

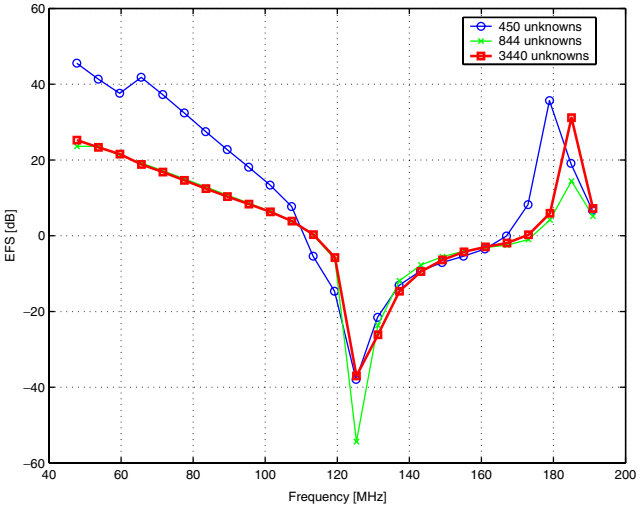

Fig. 11 Shielding efficiency of the hollow sphere with aperture—measured in the center of the sphere

- for wave number $\kappa = 1\mathrm{m}^{-1}$: monotone dependence of strength of transmitted field, starting from 0° (incident plane wave perpendicular to the aperture) to 90° (incident plane wave parallel to the aperture).
- for wave number $\kappa = 2.75\,\mathrm{m}^{-1}$ corresponding to a frequency close to the first resonance of the sphere: the coupling into the sphere no longer depends monotonically on the incidence angle.

6.2 Metallic rectangular container, partially covered, filled with sea water

The second geometry considered was a metallic rectangular container filled with sea water. The upper part is partially covered with a metallic lid as can be seen in figure Fig. 14.

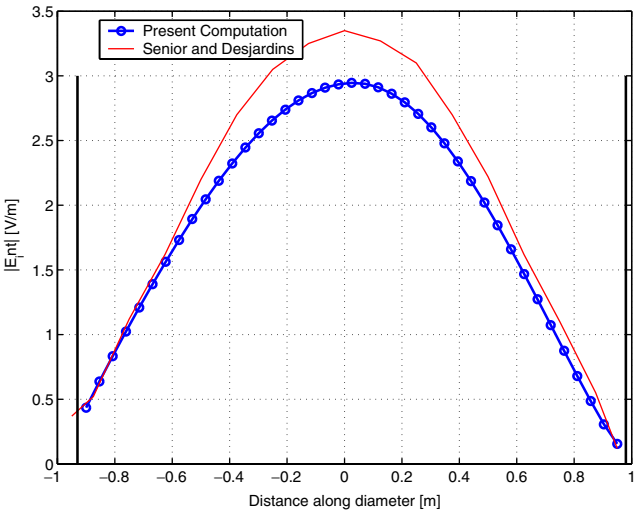

Fig. 12 Sphere: transmitted field along a diameter inside the sphere: comparison with [33] (The left vertical line denote the aperture and the right vertical line denote the end of the interval on which transmitted field was evaluated)

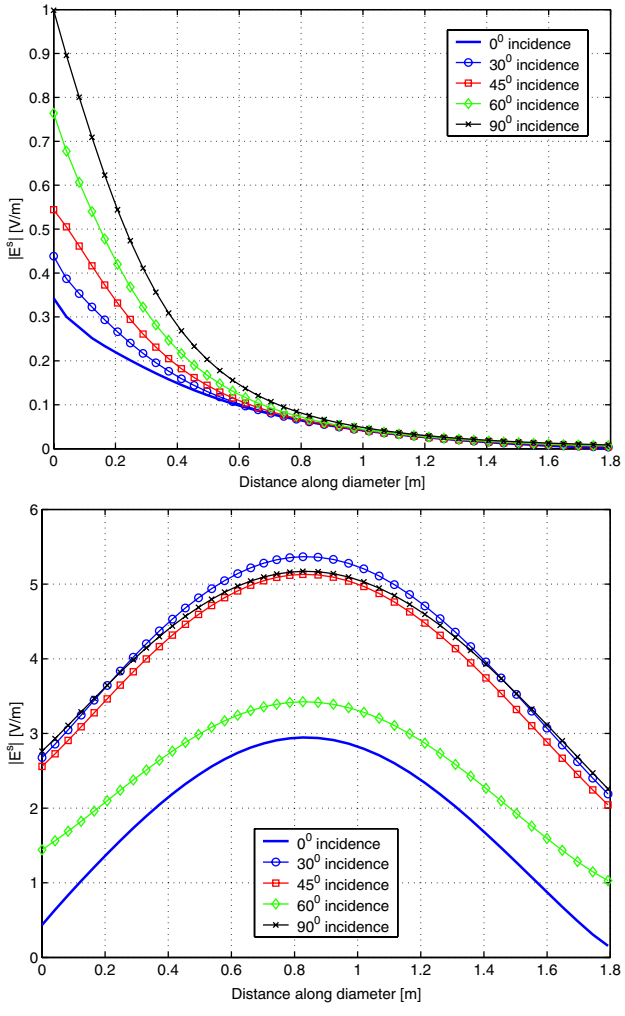

Fig. 13 Sphere: transmitted field along a diameter perpendicular to the aperture for various incidence angles of the plane wave excitation. Left: wave number $\kappa = 1\,\mathrm{m}^{-1}$, right: wave number $\kappa = 2.75\,\mathrm{m}^{-1}$

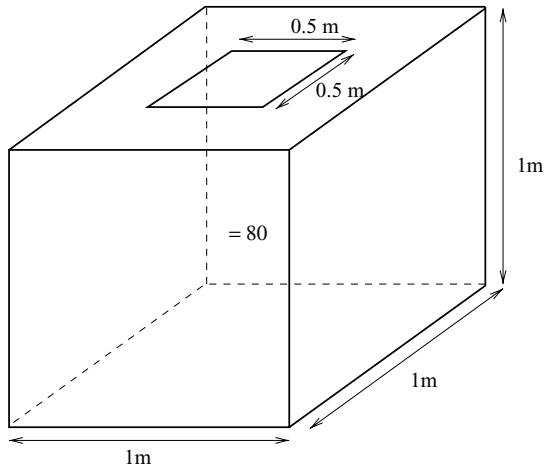

Fig. 14 Sketch of the geometry for the metallic container filled with sea water

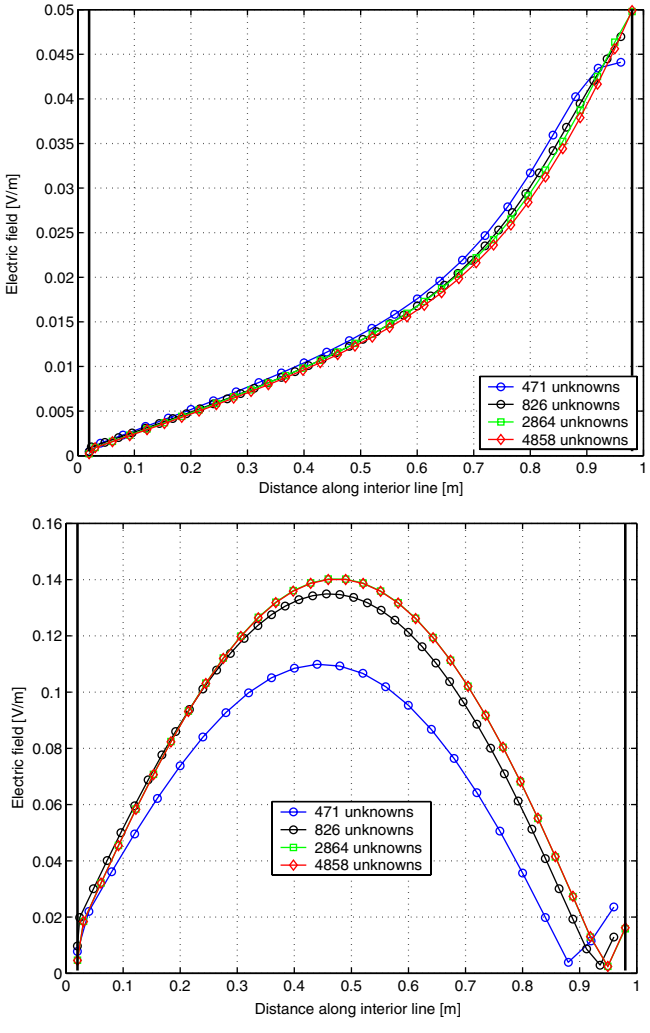

Fig. 15 Influence of mesh refinement on accuracy of solution for a metallic container filled with sea water. Left: wave number $\kappa = 3\mathrm{m}^{-1}$, right: wave number $\kappa = 4.5\,\mathrm{m}^{-1}$

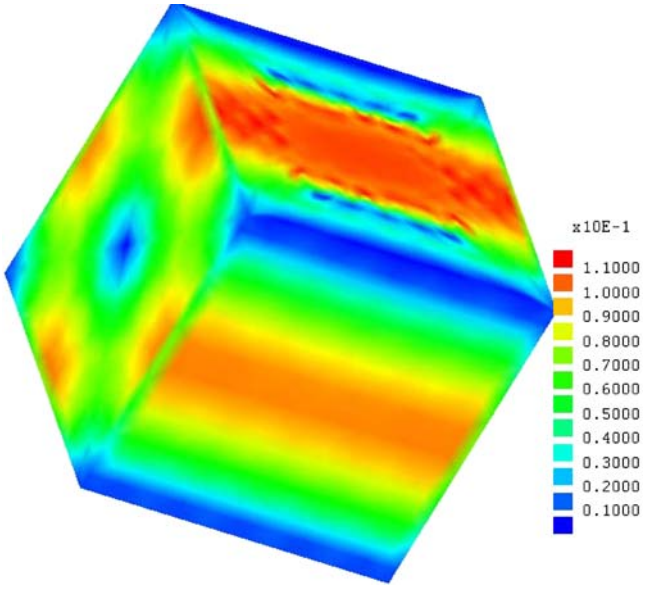

Fig. 16 Container: modulus of inner tangential magnetic field [A/m]. Wave number $\kappa = 4.5\,\mathrm{m}^{-1}$

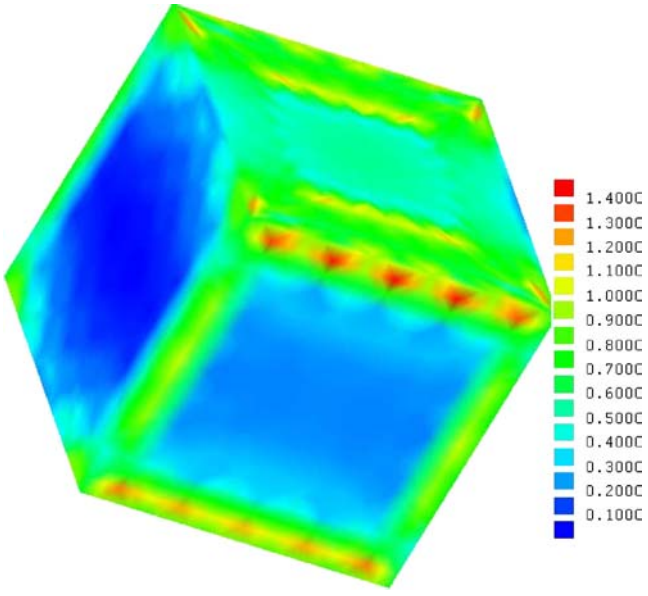

Fig. 17 Container: modulus of outer tangential magnetic field [A/m]. Wave number $\kappa = 4.5\,\mathrm{m}^{-1}$

The dielectric constant of the water was assumed to equal $\epsilon_s = 80\epsilon_0$. This leads to a situation beyond the scope of the EFIE.

A convergence study on four meshes ranging from very coarse (471 unknowns) to fine (4858 unknowns) is reported in Fig. 15 ($\kappa = 1\,\mathrm{m}^{-1}$). Obviously, away from any resonance frequencies, the solution on the coarse meshes is satisfactory already, whereas on a resonance frequency fine meshes yield significantly better results.

Plots of the electromagnetic field on the surface of the cube are presented in Figs. 16–17. Field singularities at edges are conspicuous. A section of the transmitted field is shown in (Fig. 18 for a wave number $\kappa = 4.5\,\mathrm{m}^{-1}$.

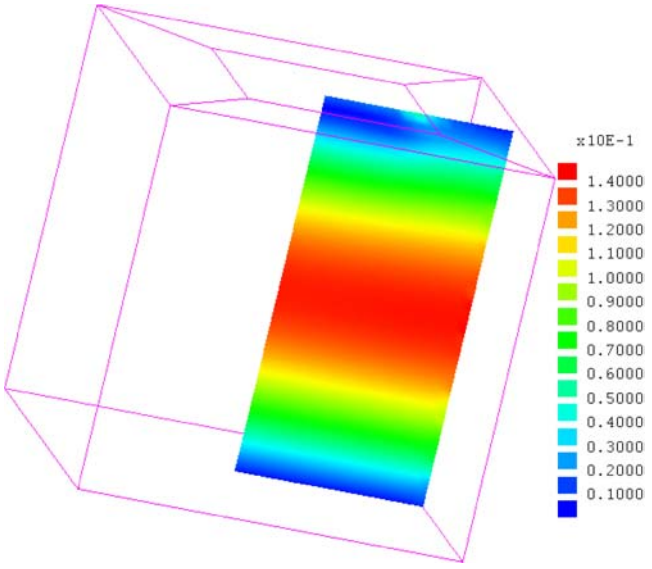

Fig. 18 Container: modulus of transmitted electric field [V/m]. Wave number $\kappa = 4.5\,\mathrm{m}^{-1}$

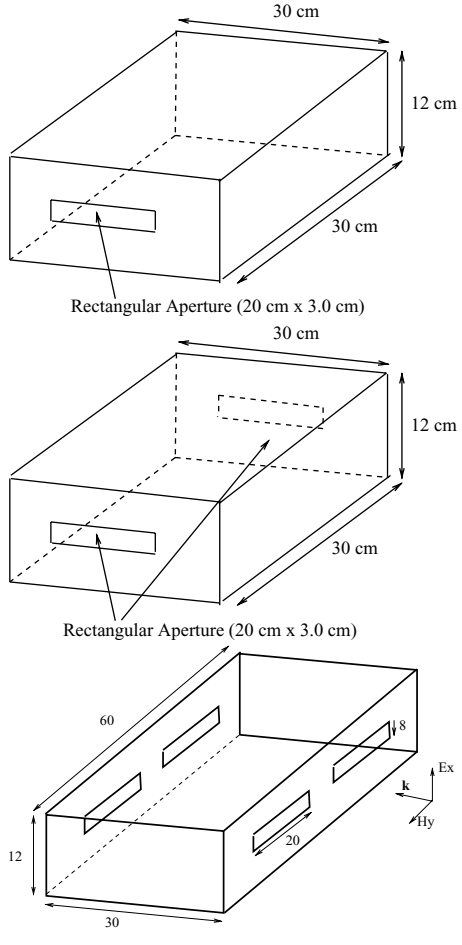

Fig. 19 Rectangular cavity with one, two, four slots

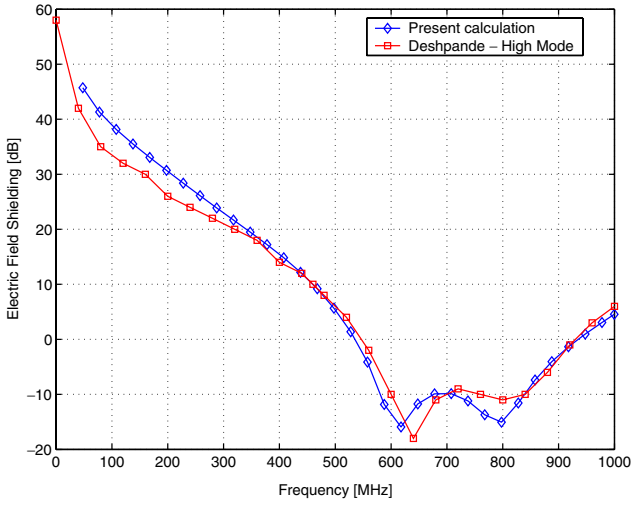

Fig. 20 Shielding efficiency of a metallic box of dimensions (30 × 12 × 30)cm, with a slot opening placed at (15, 6, 0)cm, measured in the center of the box

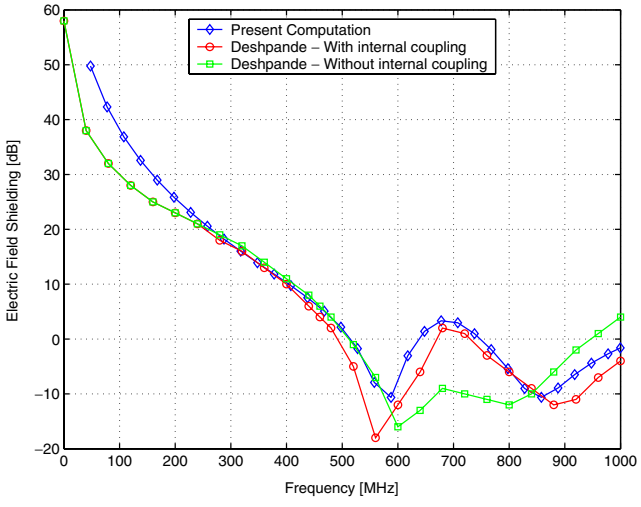

Fig. 21 Shielding efficiency of a metallic box of dimensions (30 × 12 × 30)cm, with two slot openings placed at (15, 6, 0)cm and (15, 6, 30)cm, respectively, measured in the center of the box

6.3 Metallic box with slots

Eventually, we tested the method for four simple geometries (rectangular cavity with PEC walls) with one, two or four thin slots, respectively, as can be seen in Fig. 19. Wave incidence is perpendicular to the slot faces and $\epsilon_s = \epsilon_0$, $\mu_s = \mu_0$.

Such configurations have been investigated before [17, 34]. We compare our method (1440 unknowns) with the results of [17] (horizontal polarization of incident wave), see Fig. 20. The shielding efficiency according to (42) is computed for the center of the box.

The rectangular cavity with two thin slots presented in Fig. 19 is also analyzed under plane wave incidence, perpendicular to the plane of the slots (situated at $z = 0$ and $z = 30$ cm). Our results (using 1470 unknowns) is compared with computations from Deshpande [17], see Fig. 21.

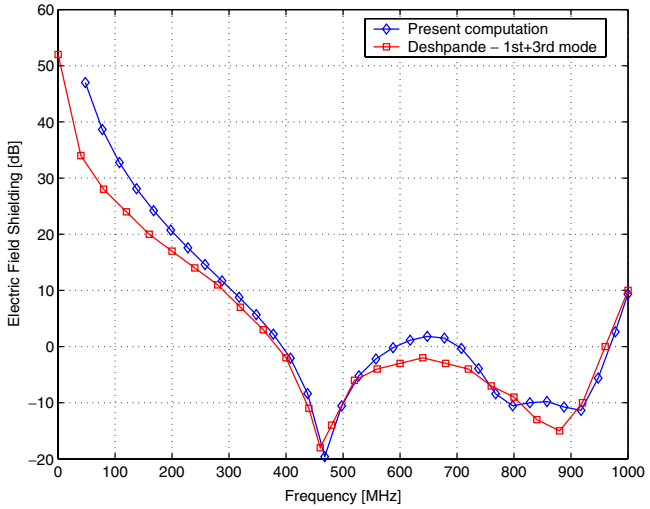

Fig. 22 Shielding efficiency of a metallic box of dimensions ($60 \times 12 \times 30$)cm, with four slot openings of (20×8)cm placed at $z = 0$ cm and $z = 30$ cm, respectively, measured in the center of the enclosure (30, 6, 15) cm

In Fig. 22 results for a PEC box excited through four slots are presented (2330 unknowns), including a comparison with [17] In general we observe a rather good agreement of the results.

References

1. Ammari, H., Nédélec, J.: Couplage éléments finis-équations intégrales pour la résolution des équations de Maxwell en milieu hétérogene, in Equations aux derivees pertielles et applications. Articles dedies a Jacques-Luois Lions, Gauthier-Villars, Paris, 19–33 (1998)
2. Brezzi, F., Fortin, M.: Mixed and Hybrid Finite Element Methods. Springer (1991)
3. Buffa, A.: Remarks on the discretization of some non-positive operators with application to heterogeneous Maxwell problems, preprint. IMATI-CNR, Pavia, Pavia, Italy (2003)
4. Buffa, A., Christiansen, S.: The electric field integral equation on Lipschitz screens: Definition and numerical approximation. Numer. Math. **94**, 229–167 (2002)
5. Buffa, A., Ciarlet, P.: On traces for functional spaces related to Maxwell's equations. Part I: An integration by parts formula in Lipschitz polyhedra., Math. Meth. Appl. Sci. **24**, 9–30 (2001)
6. Buffa, A., Ciarlet, P.: On traces for functional spaces related to Maxwell's equations. Part II: Hodge decompositions on the boundary of Lipschitz polyhedra and applications. Math. Meth. Appl. Sci. **24**, 31–48 (2001)
7. Buffa, A., Costabel, M., Sheen, D.: On traces for **H**(**curl**, Ω) in Lipschitz domains. J. Math. Anal. Appl. **276**, 845–867 (2002)
8. Buffa, A., Hiptmair, R.: Galerkin boundary element methods for electromagnetic scattering, in Topics in Computational Wave Propagation. In: M., Davis, P., Duncan, D., Martin, P., Rynne, B. (eds.), Direct and inverse Problems, Ainsworth, vol. 31 of Lecture Notes in Computational Science and Engineering, pp. 83–124. Springer, Berlin (2003)
9. Buffa, A., Hiptmair, R., von Petersdorff, T., Schwab, C.: Boundary element methods for Maxwell equations on Lipschitz domains. Numer. Math. **95** 459–485 (2003) Published online (DOI 10.1007/s00211-002-0407-z).
10. Cessenat, M.: Mathematical Methods in Electromagnetism, vol. 41 of Advances in Mathematics for Applied Sciences, World Scientific, Singapore (1996)
11. Christiansen, S.: Discrete Fredholm properties and convergence estimates for the electric field integral equation. Math. Comp. (2003). Published online July 1, 2003
12. Colton, D., Kress, R.: Inverse Acoustic and Electromagnetic Scattering Theory 2nd (ed.), vol. 93 of Applied Mathematical Sciences, Springer, Heidelberg, (1998)
13. Costabel, M.: Symmetric methods for the coupling of finite elements and boundary elements. In: Brebbia, C., Wendland, W., Kuhn, G. (eds.). Boundary Elements IX, pp. 411–420. Springer-Verlag, Berlin (1987)
14. Costabel, M., Dauge, M.: Maxwell and Lamé eigenvalues on polyhedra. Math. Methods Appl. Sci. **22**, 243–258 (1999)
15. de La Bourdonnaye, A.: Some formulations coupling finite element amd integral equation method for Helmholtz equation and electromagnetism. Numer. Math. **69**, 257–268 (1995)
16. Demkowicz, L.: Asymptotic convergence in finite and boundary element methods: Part 1, Theoretical results. Comput. Math. Appl. **27**, 69–84 (1994)
17. Deshpande, M.: Electromagnetic field penetration studies. Report CR-2000-210297, NASA (2000)
18. Hackbusch, W., Sauter, S.: On numerical cubatures of nearly singular surface integrals arising in BEM collocation. Computing **52**, 139–159 (1994)
19. Harrington, R.: Time-Harmonic Electromagnetic Fields. McGraw-Hill, New York (1961)
20. Hazard, C., Lenoir, M.: On the solution of time-harmonic scattering problems for Maxwell's equations. SIAM J. Math. Anal. **27**, 1597–1630 (1996)
21. Herschlenin, A., von Hagen, J., Wiebeck, W.: A generalized integral equation formulation for mixed dielectric-PEC scatterers. Radio Science **37**, 1058–1069 (2002)
22. Hiptmair, R.: Finite elements in computational electromagnetism, Acta Numerica. **11**, 237–339 (2002)
23. Hiptmair, R.: Coupling of finite elements and boundary elements in electromagnetic scattering. SIAM J. Numer. Anal. **41**, 919–944 (2003)
24. Jones, R., Shumpert, T.: Surface currents and rcs of a spherical shell with a circular aperture. IEEE Trans. Ant. Prop. **28**, 128–132 (1980),
25. Nédélec, J.: Mixed finite elements in $\mathbb{R}^3$. Numer. Math. **35**, 315–341 (1980)
26. Nédélec, J.-C.: Acoustic and Electromagnetic Equations: Integral Representations for Harmonic Problems, vol. 44 of Applied Mathematical Sciences. Springer-Verlag, Berlin (2001)
27. Rao, S., Wilton, D., Glisson, A.: Electromagnetic scattering by surfaces of arbitrary shape. IEEE Trans. Antennas and Propagation. **30**, 409–418 (1986)
28. Reissel, M.: On a transmission boundary-value problem for the time-harmonic Maxwell equations without displacement currents. SIAM J. Math. Anal. **24**, 1440–1457 (1993)
29. Saad, Y.: Iterative Methods for Sparse Linear Systems. PWS Publishing Co. (1995)
30. Sauter, S., Schwab, C.: Quadrature for hp-galerkin BEM in $\mathbb{R}^3$, Numer. Math. **78**, 211–258 (1997)
31. Sauter, S., Schwab, C.: Randelementmethoden. BG Teubner Stuttgart (2004)
32. Schuman, H., Warren, D.L.: Aperture coupling in bodies of revolution. IEEE Trans. Ant. Prop. **26**, 778–783 (1978)
33. Senior, T., Desjardins, G.: Electromagnetic field penetration into a spherical cavity. IEEE Trans. on Electromagnetic Compatibility. **16**, 205–208 (1974)
34. Siah, E., Yang, T., Sertel, K., Volakis, J.: Electromagnetic analysis and shielding of slots on resonant and non-resonant realistic structures with MLFMM. In Proceedings of 2002 IEEE Antennas and Propagation Symposium, vol. II, pp. 423–426. San Antonio, TX (2002)

35. von Petersdorff, T.: Boundary integral equations for mixed Dirichlet, Neumann and transmission problems. Math. Meth. Appl. Sci. **11**, 185–213 (1989)
36. Wang, T., Harrington, R., Mautz, J.: Electromangetic scattering from and transmisstion through arbitrary apertures in conducting bodies. IEEE Trans Antennas Propagation **38**, 1805–1814 (1990)
37. Wilton, D.: Review of current status and trends in the use of integral euqations in computational electromagnetics, Electromagneetics **12**, 287–341 (1992)